

Wireless Resource Optimization in Hybrid Semantic/Bit Communication Networks

Le Xia, *Graduate Student Member, IEEE*, Yao Sun, *Senior Member, IEEE*,
Dusit Niyato, *Fellow, IEEE*, Lan Zhang, *Member, IEEE*, and Muhammad Ali Imran, *Fellow, IEEE*

Abstract—Recently, semantic communication (SemCom) has shown great potential in significant resource savings and efficient information exchanges, thus naturally introducing a novel and practical cellular network paradigm where two modes of SemCom and conventional bit communication (BitCom) coexist. Nevertheless, the involved wireless resource management becomes rather complicated and challenging, given the unique background knowledge matching and time-consuming semantic coding requirements in SemCom. To this end, this paper jointly investigates user association (UA), mode selection (MS), and bandwidth allocation (BA) problems in a hybrid semantic/bit communication network (HSB-Net). Concretely, we first identify a unified performance metric of message throughput for both SemCom and BitCom links. Next, we specially develop a knowledge matching-aware two-stage tandem packet queuing model and theoretically derive the average packet loss ratio and queuing latency. Combined with practical constraints, we then formulate a joint optimization problem for UA, MS, and BA to maximize the overall message throughput of HSB-Net. Afterward, we propose an optimal resource management strategy by utilizing a Lagrange primal-dual transformation method and a preference list-based heuristic algorithm with polynomial-time complexity. Numerical results not only demonstrate the accuracy of our analytical queuing model, but also validate the performance superiority of our proposed strategy compared with different benchmarks.

Index Terms—Hybrid semantic/bit communication networks, mode selection, user association, bandwidth allocation, semantic data packet queuing analysis.

I. INTRODUCTION

SEMANTIC communication (SemCom) has recently attracted widespread attention as an emerging communication paradigm, promising to significantly alleviate the scarcity of wireless resources in next-generation cellular networks [1]. By embedding cutting-edge sophisticated deep learning (DL) models into terminal devices, SemCom is capable of providing mobile users (MUs) with a variety of high-quality, large-capacity, and multimodal services, including typical multimedia content (e.g., text [2], image [3], and video streaming [4]) and artificial intelligence-generated content (AIGC) [5]. Different from the conventional bit communication (BitCom)

mode that aims at the precise reception of transmitted bits, SemCom focuses more on the accurate delivery of the true meanings implied in source messages.

Specifically, a semantic encoder deployed in the transmitter first filters out redundant content of the source information and extracts the core semantics that require fewer bits for transmission. After necessary channel encoding and decoding, the original meanings are accurately interpreted and restored from the received bits via a semantic decoder, even with intolerable bit errors in data propagation. Notably, either the semantic encoding or decoding is executed based on background knowledge pertinent to the delivered messages,¹ and the higher the knowledge-matching degree between transceivers, the lower the semantic ambiguity in recovered meanings [6]. Consequently, it is envisioned that the introduction of SemCom can ensure efficient and reliable information exchanges and save considerable spectrum resources.

Recap the recent advancement of SemCom, there have been some noteworthy related works propelling both its information-theoretic and link-level systematic modelings. In [7] and [8], Bao *et al.* quantitatively measured semantic entropy by first proposing a semantic channel-coding theorem, which is based on the information logical probability defined by Carnap and Bar-Hillel in [9]. Besides, Liu *et al.* [10] identified the semantic rate-distortion function by leveraging the intrinsic state and extrinsic observation of information in a memoryless source case. As for the semantic transceiver design, Xie *et al.* [2] devised a Transformer-enabled end-to-end SemCom system for reliable text transmission, and then upgraded this system to be lightweight in [11]. Moreover, Xia *et al.* [4] presented a mobile virtual reality SemCom framework that can guarantee high-performance semantic extraction and frame recovery for delivering 360° video streaming.

In parallel, several other preliminary studies related to SemCom have further investigated the wireless resource management issue from a networking perspective. Powered by deep reinforcement learning algorithms, Zhang *et al.* [3] adopted a dynamic resource allocation scheme to maximize the long-term transmission efficiency in task-oriented SemCom networks. In [12], Yang *et al.* exploited a probability graph and a rate splitting method to achieve energy-efficient SemCom networks on both transmission and computation. Likewise, a quantum key distribution-secured resource management framework was considered by Kaewpuang *et al.* [13]

¹In DL-driven SemCom systems, the background knowledge is deemed training data samples serving a certain class of learning tasks [2], [3]. Relevant research is beyond the scope of this paper and will not be discussed in-depth.

Le Xia, Yao Sun (*Corresponding author: Yao Sun.*), and Muhammad Ali Imran are with the James Watt School of Engineering, University of Glasgow, Glasgow G12 8QQ, UK (e-mail: l.xia.2@research.gla.ac.uk; {Yao.Sun, Muhammad.Imran}@glasgow.ac.uk).

Dusit Niyato is with the College of Computing and Data Science, Nanyang Technological University, Singapore 639798 (e-mail: dniyato@ntu.edu.sg).

Lan Zhang is with the Department of Electrical and Computer Engineering, Clemson University, Clemson, South Carolina 29634, USA (e-mail: lan7@clemson.edu).

for the edge devices communicating semantic information. Apart from these, Xia *et al.* [6] specially developed a bit-rate-to-message-rate transformation function along with a new semantic-aware metric called system throughput in message to jointly optimize user association (UA) and bandwidth allocation (BA) problems in SemCom-enabled cellular networks.

While most research works focus solely on SemCom, there is still a missing investigation on wireless resource optimization in a more practical scenario, namely *hybrid semantic/bit communication networks* (HSB-Nets), where both SemCom and BitCom modes are available for multiple MUs. As a matter of fact, the necessity of emphasizing the HSB-Net lies in the current colossal infrastructures and user groups in BitCom that cannot be completely replaced at one time, while taking into account the unprecedented potential and superiorities of SemCom in terms of efficient information exchanges and wireless resource savings. Therefore, the HSB-Net will be an inevitable and long-lasting intermediate network paradigm during the future evolution of wireless cellular networks, and is also expected to yield a host of benefits, such as flexible and targeted service provisioning, adequate resource utilization, and satisfactory user experience on semantic performance.

Nevertheless, since SemCom typically requires more data processing time but produces higher semantic performance than BitCom at each transceiver, choosing a proper mode for each MU should be rather complicated and challenging. Most uniquely, the varying degrees of background knowledge matching among MUs can also affect the amount of allocated bandwidth in combination with different channel conditions. As such, if aiming at high semantic fidelity and low latency for a large-scale HSB-Net, we are encountering the following three fundamental challenges in resource management:

- *Challenge 1: How to unify performance metrics for both SemCom and BitCom in the HSB-Net?* Given the core mechanism of meaning delivery in SemCom, traditional metrics in BitCom, like bit rate or bit throughput, are evidently no longer applicable to the SemCom links. Especially in such a hybrid scenario, it becomes necessary to align SemCom and BitCom to the same assessment basis to facilitate subsequent performance comparisons or overall network optimization, which raises the first nontrivial point.
- *Challenge 2: How to mathematically characterize the unique semantic-coding process in SemCom when combined with bit transmission?* Note that SemCom involves an extra semantic-coding process compared with BitCom before the bit data transmission at each link, which can be characterized from a packet-queuing perspective. In the semantic-coding process, due to diverse knowledge-matching degrees among different SemCom-enabled MUs, semantic data packet interpretation rates can vary [14], thereby resulting in distinct queuing delay and reliability performance. Combined with the subsequent indispensable packet-transmission queuing process, all of these constitute the second difficulty.
- *Challenge 3: How to determine the best communication mode for each MU with the joint consideration of UA and BA to optimize overall network performance?* Generally,

each MU can select only one of the SemCom and BitCom modes at a time during the UA process, subject to its current knowledge-matching degree, channel condition, desired service quality, as well as latency and reliability budgets. Such a new mode selection (MS) problem, coupled with inherent practical constraints such as limited bandwidth resources and the single-base station (BS) association requirement, poses the third challenge, i.e., seeking an optimal resource management strategy for the UA, MS, and BA to jointly optimize overall network performance in the HSB-Net.

In response to the challenges outlined above, in this paper, we systematically investigate the UA, MS, and BA problems in the uplink of the HSB-Net and correspondingly propose an optimal strategy with the awareness of unique SemCom characteristics. Simulation results not only demonstrate the accuracy of our theoretical analysis for semantic data packet queuing, but also showcase the performance superiority of the proposed resource management solution in terms of realized message throughput compared with four benchmarks. Accordingly, our main contributions are summarized as follows:

- We unify the performance metrics for both SemCom and BitCom links by introducing the bit-rate-to-message-rate transformation mechanism to measure their respective achievable message throughputs. In this regard, the stochasticity of knowledge matching degree and channel state are particularly taking into account over different time slots. Correspondingly, we then formulate an optimization problem to maximize the time-averaged overall message throughput of the HSB-Net by jointly correlating the UA, MS, and BA-related indicators. These first address the aforementioned *Challenge 1*.
- We specially model a two-stage tandem queue for each SemCom-enabled MU to capture the entire queuing process of its locally generated semantic packets, which fully incorporates the semantic coding and knowledge-matching characteristics with the traditional packet transmission. On this basis, the steady-state average packet loss ratio and queuing delay in both SemCom and BitCom cases are then mathematically derived to post the reliability and latency requirements in subsequent optimization. The contribution directly addresses *Challenge 2*.
- We theoretically prove the monotonicity of allocated bandwidth with respect to reliability and latency, and then develop an efficient resource management strategy to jointly solve the UA, MS, and BA problems with polynomial-time complexity. Specifically, the minimum bandwidth threshold is first fixed for each SemCom and BitCom link, following by a Lagrange primal-dual method and a preference list-based heuristic algorithm to finalize the UA and MS solutions. Afterward, the optimal BA strategy is further obtained by reallocating the remaining bandwidth of each BS to all its associated MUs. In this way, *Challenge 3* is finally well tackled.

The remainder of this paper is organized as follows. Section II first introduces the system model of HSB-Net. Then, the queuing analysis for both SemCom and BitCom cases are

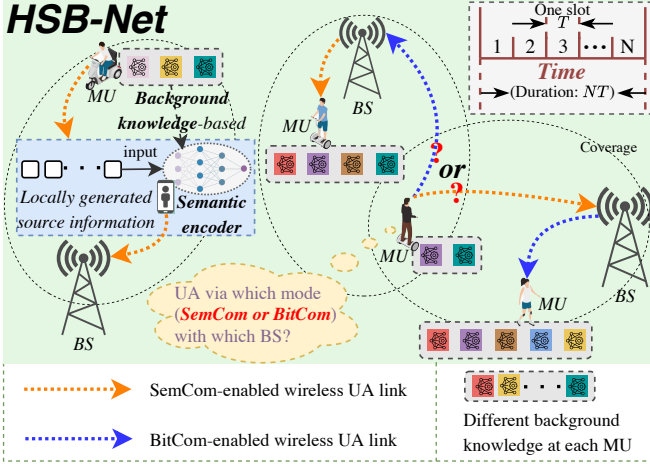


Fig. 1. The HSB-Net scenario involving UA, MS, and BA in one time block.

presented, and the corresponding joint resource management problem is formulated in Section III. In Section IV, we illustrate the proposed optimal UA, MS, and BA strategy. Numerical results are demonstrated and discussed in Section V, followed by the conclusions in Section VI.

II. SYSTEM MODEL

A. HSB-Net Scenario

Consider an HSB-Net scenario as depicted in Fig. 1, the total of U MUs are distributed within the coverage of S BSs, where two communication modes of SemCom and BitCom are available for all MUs, while each MU can only select one mode and be associated with one BS at a time. Herein, let $x_{ij} \in \{0, 1\}$ denote the binary UA indicator, where $x_{ij} = 1$ means that MU $i \in \mathcal{U} = \{1, 2, \dots, U\}$ is associated with BS $j \in \mathcal{J} = \{1, 2, \dots, J\}$, and $x_{ij} = 0$ otherwise. Besides, we specially define the binary MS indicator as $y_{ij} \in \{0, 1\}$, where $y_{ij} = 1$ represents that the SemCom mode is selected for the link between MU i and BS j , and $y_{ij} = 0$ indicates that the BitCom mode is selected.² Meanwhile, the amount of bandwidth resource that BS j assigns to MU i is denoted as z_{ij} , while the total bandwidth budget of BS j is denoted as Z_j . Moreover, time is equally partitioned into N consecutive time slots, each with the same duration length T .

B. Network Performance Metric

For the wireless propagation model, first let $\gamma_{ij}(t)$ denote the signal-to-interference-plus-noise ratio (SINR) of the link between MU i and BS j at time slot t , $t = 1, 2, \dots, N$. Note that $\gamma_{ij}(t)$ is assumed to be an independent and identically distributed (i.i.d.) random variable for different slots but remain constant during one slot [15], [16]. Since the conveyed message itself becomes the sole focus of precise reception in SemCom rather than traditional transmitted bits in BitCom, we proceed with the performance metric developed in our previous work [6] to measure the message rate for each

²It is worth pointing out that y_{ij} is applicable to be an effective MS indicator only when $x_{ij} = 1, \forall (i, j) \in \mathcal{U} \times \mathcal{J}$.

SemCom-enabled MU via employing a bit-rate-to-message-rate (B2M) transformation function. To be specific, the B2M function is to output the semantic channel capacity (i.e., the achievable message rate in units of messages per unit time, *msg/s*) from input traditional Shannon channel capacity (i.e., the achievable bit rate in units of bits per unit time, *bit/s*) under the discrete memoryless channel.³ If in an ideal condition, i.e., the information source and destination have identical semantic reasoning capability and equivalent background knowledge, the B2M function can be approximated as linear. However, the B2M can also involve stochastic variables in the case of knowledge mismatch, resulting in the presentation of random message rates. Given this, let $\mathfrak{R}_{ij}(\cdot)$ denote the B2M function of the SemCom link between MU i and BS j , its instantaneous achievable message rate in time slot t should be

$$M_{ij}^S(t) = \beta_i(t) \mathfrak{R}_{ij}(z_{ij} \log_2(1 + \gamma_{ij}(t))). \quad (1)$$

Here, $\beta_i(t)$ represents the knowledge-matching degree between MU i and its communication counterpart at slot t , which is an i.i.d. random Gaussian variable ranging from 0 to 1 [6], having mean τ_i . In more detail, the rationale behind introducing $\beta_i(t)$ is that for any MU in the knowledge-mismatching state, only a proportion of all its messages transformed from $\mathfrak{R}_{ij}(\cdot)$ in each slot can be interpreted effectively, and this proportion is equivalent to its knowledge-matching degree. Together with the fact that the generation of source information is generally modeled as a stochastic process [10], therefore, $\beta_i(t)$ is deemed as a random variable.

Likewise, for each MU that selects the BitCom mode for UA, we assume that there is an average B2M transformation ratio,⁴ in order to measure the network performance with a message-related metric unified with SemCom. Denoting the B2M transformation coefficient of the BitCom-based link between MU i and BS j as ρ_{ij} , the instantaneous achievable message rate of this link in slot t is given by

$$M_{ij}^B(t) = \rho_{ij} z_{ij} \log_2(1 + \gamma_{ij}(t)), \quad 0 < \rho_{ij} < 1. \quad (2)$$

As such, if taking into account both SemCom (i.e., $y_{ij} = 1$) and BitCom (i.e., $y_{ij} = 0$) cases, we obtain the time-averaged message rate of each link as

$$M_{ij} = \frac{1}{N} \sum_{t=1}^N [y_{ij} M_{ij}^S(t) + (1 - y_{ij}) M_{ij}^B(t)]. \quad (3)$$

C. Queuing Model

In this work, we focus on the differences in queuing models between SemCom and BitCom during data uplink transmission, where the queuing delay is employed as the latency metric to characterize the average sojourn time of a data

³The semantic channel capacity with respect to B2M is derived from a semantic information-theoretical perspective, which is beyond the scope of this paper and thus will not be discussed in-depth. More technical details can be found in [6] and [7].

⁴This assumption is justified since the source-and-channel coding of BitCom for source information typically follows prescribed codebooks, and the variable length coding is adopted [5], [17]. Hence, based on each link's known channel state information, the proportion of messages that can be effectively decoded from a certain amount of transmitted bits can be averaged.

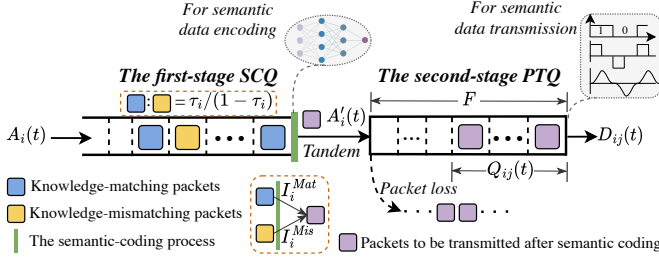


Fig. 2. The two-stage tandem queue model at each SemCom-enabled MU.

packet in the queue buffer at each MU in the HSB-Net. Unlike existing studies that consider only packet queuing during the channel-coding process in BitCom [18]–[21], the queuing delay at a SemCom-enabled MU should take into account the newly introduced semantic-coding process in combination with traditional packet transmission, as shown in Fig. 2. To this end, we first provide the following definition for clarity.

Definition 1. A SemCom-enabled MU has a two-stage tandem queue,⁵ named *Semantic-Coding Queue (SCQ)* and *Packet-Transmission Queue (PTQ)*. As for a BitCom-enabled MU, only one PTQ is considered for its packet uplink transmission.

To preserve the generality, the SCQ is assumed with infinite-size memory to handle all locally generated SemCom services, while the PTQ has a finite-size buffer that can accommodate up to F data packets to align with practical resource limitations and scheduling.⁶ Moreover, the packets in both SCQ and PTQ are queued in a first-come-first-serve manner.

Based on the above, if a Poisson arrival process with average rate λ_i (in *packets/s*) of initial data packet generation is assumed for each MU i ($\forall i \in \mathcal{U}$), the number of arrival packets during slot t , denoted as $A_i(t)$, has the probability mass function (PMF) as follows:

$$\Pr \{A_i(t) = k\} = \frac{(\lambda_i T)^k}{k!} \exp(-\lambda_i T), \quad k = 0, 1, 2, \dots \quad (4)$$

For the PTQ in both SemCom and BitCom cases, its packet departure rate depends on the number of packets sent out from MU i to BS j ($\forall j \in \mathcal{J}$) during slot t , denoted as $D_{ij}(t)$, which has the PMF as

$$\begin{aligned} \Pr \{D_{ij}(t) = k\} &= \Pr \left\{ \left\lfloor \frac{Tz_{ij} \log_2(1 + \gamma_{ij}(t))}{L} \right\rfloor = k \right\} \\ &= \Pr \left\{ \gamma_{ij}(t) \leq 2^{\frac{(k+1)L}{Tz_{ij}}} - 1 \right\} - \Pr \left\{ \gamma_{ij}(t) \leq 2^{\frac{kL}{Tz_{ij}}} - 1 \right\}. \end{aligned} \quad (5)$$

Here, $\lfloor \cdot \rfloor$ is the floor function that outputs the largest integer less than or equal to the input value, and all packets have the same size of L bits, $k = 0, 1, 2, \dots$. Clearly, given any reasonable probability distribution approximation of the SINR $\gamma_{ij}(t)$ (e.g., Gaussian distribution [16] or generalized

⁵A two-stage tandem queue implies that the output of the first queue becomes the input of the second, and the packet processing in the two queues is independent of each other [21], [22].

⁶Note that the SCQ can also be modeled with a finite-size buffer whose queuing latency is derived similarly to that of the PTQ. Likewise, the above rationale applies to the PTQ as well.

Gamma distribution [23]), applying its cumulative distribution function (CDF) directly yields the close-form expression of (5). Besides, it is noteworthy that the obtained PMF of $D_{ij}(t)$ should be independent of time slot index t , as the randomness of each physical link's SINR is generally t -independent [15].

Next, we model the packet departure of SemCom-enabled SCQ and the packet arrival of SemCom-enabled PTQ, respectively. As mentioned earlier, each data packet generated at a SemCom-enabled sender MU requires a certain type of background knowledge, resulting in either a knowledge-matching or knowledge-mismatching state with its receiver. For illustration, let I_i^{Mat} denote the semantic-coding time required by a knowledge-matching packet with mean $1/\mu_i^{Mat}$ (in *s/packet*), and let I_i^{Mis} denote the semantic-coding time required by a knowledge-mismatching packet with mean $1/\mu_i^{Mis}$ ($\mu_i^{Mat} > \mu_i^{Mis}$ in practice⁷). Without loss of generality, I_i^{Mat} and I_i^{Mis} are assumed to be two exponential random variables independent of each other, which are determined by the specific semantic computing capability available at the MU i 's terminal device. Having these, it is seen that the overall service time distribution of packets at SCQ should be treated as a general distribution [14]. Let us denote the average packet queuing latency of SCQ at each SemCom-enabled MU i by $\delta_i^{S_i}$, which will be analyzed in detail in the next section.

As for the number of packets arriving at the SemCom-enabled PTQ in slot t , denoted by $A'_i(t)$, it should exactly be the number of packets leaving its tandem SCQ in the same slot, according to the two-stage tandem structure in Definition 1. Meanwhile, it is not difficult to deduce that the knowledge-matching packets leaving the SCQ follow a Poisson process with mean μ_i^{Mat} , while the knowledge-mismatching packets leave as a Poisson process with mean μ_i^{Mis} . The former event occurs with probability τ_i and the latter happens with probability $(1 - \tau_i)$. As such, $A'_i(t)$ should still satisfy the Poisson distribution with a PMF of

$$\Pr \{A'_i(t) = k\} = \frac{(\lambda'_i T)^k}{k!} \exp(-\lambda'_i T), \quad k = 0, 1, 2, \dots, \quad (6)$$

where λ'_i is the average arrival rate (in *packets/s*), given as

$$\lambda'_i = \tau_i \mu_i^{Mat} + (1 - \tau_i) \mu_i^{Mis}. \quad (7)$$

Considering the limited buffer size F of PTQ, we further assume that in any t , the packets to be transmitted leave the queue first and then the arriving packets enter it. Hence, the evolution of its queue length between two consecutive slots is

$$Q_{ij}(t+1) \triangleq \min \{ \max \{ Q_{ij}(t) - D_{ij}(t), 0 \} + A'_i(t), F \}, \quad (8)$$

where $Q_{ij}(t)$ denotes the queue length of PTQ for the link between MU i and BS j at slot t , $t = 1, 2, \dots, N - 1$.

Note that those packets arriving at a fully-loaded PTQ in each slot will be blocked and dropped, which can affect achievable communication reliability and message rate performance. Accordingly, let θ_{ij}^S and θ_{ij}^B denote the average packet

⁷Notice that the content in knowledge-mismatching packets necessarily requires more computational resources and processing time for accurate contextual reasoning and interpretation, due to the use of more sophisticated semantic-coding networks or the knowledge-sharing method, etc [24].

loss ratio of SemCom-enabled PTQ and BitCom-enabled PTQ, respectively, and each represents the proportion of packets failed to be delivered to all arriving packets. Likewise, let $\delta_{ij}^{S_2}$ and δ_{ij}^B denote the average packet queuing latency of SemCom-enabled PTQ and BitCom-enabled PTQ, respectively. Combined with the $\delta_{ij}^{S_1}$ defined before, we obtain the overall average queuing latency of the link between SemCom-enabled MU i and BS j as $\delta_{ij}^S = \delta_i^{S_1} + \delta_{ij}^{S_2}$.

When considering both SemCom (i.e., $y_{ij} = 1$) and BitCom (i.e., $y_{ij} = 0$), the average queuing latency experienced by the link between any MU i and BS j should be

$$\delta_{ij} = y_{ij}\delta_{ij}^S + (1 - y_{ij})\delta_{ij}^B. \quad (9)$$

Similarly, the average packet loss ratio that indicates the communication reliability of the link is found by

$$\theta_{ij} = y_{ij}\theta_{ij}^S + (1 - y_{ij})\theta_{ij}^B. \quad (10)$$

In the subsequent section, we elaborate the derivations for the mathematical expressions of $\delta_{ij}^{S_1}$, $\delta_{ij}^{S_2}$, and θ_{ij}^S . Recalling the BitCom-enabled PTQ model and the SemCom-enabled PTQ model, it is seen that their sole distinction lies in their packet arrival processes, in which the former follows (4) and the latter follows (6). Therefore, δ_{ij}^B and θ_{ij}^B can be easily derived using the similar procedure as for $\delta_{ij}^{S_2}$ and θ_{ij}^S .

III. QUEUING ANALYSIS AND PROBLEM FORMULATION

A. Queuing Analysis for SCQ and PTQ

First for the SemCom-enabled SCQ, it should be noted that the average proportion of knowledge-matching packets to the total number of packets in the queue is exactly equal to the average knowledge-matching degree τ_i between MU i and its receiver.⁸ Combined with the general distribution conclusion obtained earlier, the average semantic-coding time of a packet in the SCQ, denoted by I_i , becomes $I_i = \tau_i I_i^{Mat} + (1 - \tau_i) I_i^{Mis}$. Since I_i^{Mat} and I_i^{Mis} are independent of each other, we have its expectation as $\mathbb{E}[I_i] = \tau_i/\mu_i^{Mat} + (1 - \tau_i)/\mu_i^{Mis}$ and its variance as $\mathbb{V}(I_i) = (\tau_i/\mu_i^{Mat})^2 + ((1 - \tau_i)/\mu_i^{Mis})^2$. Owing to the Markovian packet arrival and general-distribution packet departure, the SCQ follows an M/G/1 system, which has been widely used to capture data traffic in wireless networks [14]. In this case, we can directly apply the *Pollaczek-Khintchine formula* [25] to calculate the steady-state average packet queuing latency of SCQ $\delta_i^{S_1}$, which is expressed in (11) as shown at the bottom of this page.⁹ It is worth further noting that either I_i^{Mat} or I_i^{Mis} in (11) is independent of time slot index t , thus $\delta_i^{S_1}$ should be deemed a constant.

⁸This observation holds true when examined on a large timescale, and it assumes that each packet has the same probability of being generated locally.

⁹Applying the Pollaczek-Khintchine formula implies a prerequisite that $\lambda_i \mathbb{E}[I_i] < 1$ must be satisfied to guarantee a steady-state M/G/1 system [26]. Therefore, we consider that in the SCQ, the packet departure rate exceeds the packet arrival rate to make its queuing latency finite and solvable.

When it comes to the SemCom-enabled PTQ, we first introduce the following proposition to characterize its steady-state queue length $Q_{ij}(t) = 0, 1, 2, \dots, k, \dots, F$ in slot t .

Proposition 1. *For each $Q_{ij}(t)$ of PTQ, it must have a solvable and unique steady-state probability vector, denoted as $\alpha_{ij} = [\alpha_{ij}^0, \alpha_{ij}^1, \dots, \alpha_{ij}^F]^T$, where α_{ij}^k represents the steady-state probability of $Q_{ij}(t) = k$ when t tends to infinity.*

Proof: Please see Appendix A. ■

From Proposition 1, the long-term average queue length of $Q_{ij}(t)$ can be obtained by computing its expectation, i.e., $\mathbb{E}[Q_{ij}(t)] = \sum_{k=0}^F k \alpha_{ij}^k$. Moreover, by combining α_{ij} with the PMFs of PTQ's packet arrival as in (6) and packet departure as in (5), the average number of packets dropped at the steady-state PTQ during any slot t , denoted by G_{ij} , can be calculated by (12) at the bottom of the next page. As its average total packet arrival rate is λ'_i , we have the steady-state average packet loss ratio of SemCom-enabled PTQ as follows:

$$\theta_{ij}^S = \frac{G_{ij}}{\lambda'_i T} = \frac{G_{ij}}{\tau_i \mu_i^{Mat} T + \mu_i^{Mis} T - \tau_i \mu_i^{Mis} T}. \quad (13)$$

Hence, the average effective packet arrival rate becomes $\lambda_i^{eff} = (1 - \theta_{ij}^S) \lambda'_i = \tau_i \mu_i^{Mat} + (1 - \tau_i) \mu_i^{Mis} - G_{ij}/T$. As such, we can apply Little's law [27] to finalize the steady-state average queuing latency of SemCom-enabled PTQ as

$$\delta_{ij}^{S_2} = \frac{\mathbb{E}[Q_{ij}(t)]}{\lambda_i^{eff}} = \frac{\sum_{k=0}^F k \alpha_{ij}^k}{\tau_i \mu_i^{Mat} + (1 - \tau_i) \mu_i^{Mis} - G_{ij}/T}. \quad (14)$$

Furthermore, to determine the expressions of BitCom-enabled average packet queuing latency δ_{ij}^B and the BitCom-enabled average packet loss ratio θ_{ij}^B , the same mathematical methods as the above can be employed, where only the PMF and mean of $A'_i(t)$ as in (6) in each relevant term need to be substituted with that of $A_i(t)$ as in (4). For brevity, the derivation details for δ_{ij}^B and θ_{ij}^B are omitted here.

B. Problem Formulation

For ease of illustration, we first define three variable sets $\mathbf{x} = \{x_{ij} \mid i \in \mathcal{U}, j \in \mathcal{J}\}$, $\mathbf{y} = \{y_{ij} \mid i \in \mathcal{U}, j \in \mathcal{J}\}$, and $\mathbf{z} = \{z_{ij} \mid i \in \mathcal{U}, j \in \mathcal{J}\}$ that consist of all possible indicators pertinent to UA, MS, and BA, respectively. Without loss of generality, the objective is to maximize the overall message throughput (i.e., the sum of the achievable message rates of all MUs) of the HSB-Net by jointly optimizing $(\mathbf{x}, \mathbf{y}, \mathbf{z})$, while subject to SemCom-relevant latency and reliability requirements alongside several practical system constraints. Notably, the message throughput metric is measured from the long-

$$\delta_i^{S_1} = \frac{\lambda_i (\mathbb{E}^2[I_i] + \mathbb{V}(I_i))}{2(1 - \lambda_i \mathbb{E}[I_i])} + \mathbb{E}[I_i] = \frac{\lambda_i \left[\tau_i (1 - \tau_i) / \mu_i^{Mat} \mu_i^{Mis} + (\tau_i / \mu_i^{Mat})^2 + ((1 - \tau_i) / \mu_i^{Mis})^2 \right]}{1 - \lambda_i \tau_i / \mu_i^{Mat} - \lambda_i (1 - \tau_i) / \mu_i^{Mis}} + \frac{\tau_i}{\mu_i^{Mat}} + \frac{1 - \tau_i}{\mu_i^{Mis}}. \quad (11)$$

term perspective as in (3). Accordingly, if denoting the mean of $\gamma_{ij}(t)$ as $\bar{\gamma}_{ij}$, we can rewrite (3) by

$$\begin{aligned}\bar{M}_{ij} &= y_{ij}\bar{M}_{ij}^S + (1 - y_{ij})\bar{M}_{ij}^B \\ &= y_{ij}\tau_i \mathfrak{R}_{ij}(z_{ij} \log_2(1 + \bar{\gamma}_{ij})) + \rho_{ij} z_{ij} (1 - y_{ij}) \log_2(1 + \bar{\gamma}_{ij}).\end{aligned}\quad (15)$$

Recalling the average queuing latency δ_{ij} as in (9) and the average packet loss ratio θ_{ij} as in (10), our joint optimization problem **P1** is now formulated as follows:

$$\mathbf{P1} : \max_{\mathbf{x}, \mathbf{y}, \mathbf{z}} \sum_{i \in \mathcal{U}} \sum_{j \in \mathcal{J}} x_{ij} \bar{M}_{ij} \quad (16)$$

$$\text{s.t.} \quad \sum_{j \in \mathcal{J}} x_{ij} = 1, \quad \forall i \in \mathcal{U}, \quad (16a)$$

$$\sum_{i \in \mathcal{U}} x_{ij} z_{ij} \leq Z_j, \quad \forall j \in \mathcal{J}, \quad (16b)$$

$$x_{ij} \delta_{ij} \leq \delta_0, \quad \forall (i, j) \in \mathcal{U} \times \mathcal{J}, \quad (16c)$$

$$x_{ij} \theta_{ij} \leq \theta_0, \quad \forall (i, j) \in \mathcal{U} \times \mathcal{J}, \quad (16d)$$

$$\sum_{j \in \mathcal{J}} x_{ij} \bar{M}_{ij} \geq M_i^o, \quad \forall i \in \mathcal{U}, \quad (16e)$$

$$x_{ij} \in \{0, 1\}, \quad y_{ij} \in \{0, 1\}, \quad \forall (i, j) \in \mathcal{U} \times \mathcal{J}. \quad (16f)$$

Constraints (16a) and (16b) mathematically model the single-BS constraint for UA and the maximum bandwidth resource constraint for BA, respectively. Constraints (16c) and (16d) ensure that the average queuing latency and the average packet loss ratio of the link between each MU and its associated BS cannot exceed their respective requirements δ_0 and θ_0 . M_i^{th} in constraint (16e) represents a minimum message rate threshold for each MU i 's association link, while constraint (16f) characterizes the binary properties of both \mathbf{x} and \mathbf{y} .

Carefully examining **P1**, it can be observed that the optimization is rather challenging due to several inevitable mathematical obstacles. First of all, **P1** is clearly an NP-hard problem involving two complicated constraints (16c) and (16d), which leads to a high-complexity solution procedure. Another nontrivial point originates from the three different optimization variables, including two integer variables (i.e., \mathbf{x} and \mathbf{y}) and one continuous variable (i.e., \mathbf{z}). In this respect, although we could first relax \mathbf{x} and \mathbf{y} to the continuous ones in a conventional manner, the problem after slack should still be nonconvex and the subsequent integer recovery may lead to severe performance compromise [28]. In full view of the above difficulties, we propose an efficient solution in the next section to solve **P1** and obtain the joint optimal strategy for the UA, MS, and BA in the HSB-Net.

IV. OPTIMAL RESOURCE MANAGEMENT IN HSB-NETS

To make **P1** tractable, each z_{ij} ($\forall (i, j) \in \mathcal{U} \times \mathcal{J}$) is first fixed to two thresholds based on both the SemCom case and the BitCom case, respectively. Next, we determine the initial UA and MS strategies by employing a Lagrange primal-dual method, and then devise a preference list-based heuristic algorithm to reach the optimality. On this basis, the BA strategy is then optimally finalized by reallocating the bandwidth of each BS to all its associated MUs while accommodating their respective identified communication modes. Finally, we present the complexity analysis of the proposed solution.

A. Strategy Determination for UA and MS

There is a minimum bandwidth amount that BS j should allocate to each of its associated SemCom-enabled MU i and BitCom-enabled MU i to simultaneously meet the preset latency, reliability, and message throughput requirements. The feasibility behind this approach is established in accordance with the following proposition.

Proposition 2. *The steady-state average packet queuing latency δ_{ij} and average packet loss ratio θ_{ij} are monotonically non-increasing w.r.t. z_{ij} given any value of y_{ij} .*

Proof: Please see Appendix B. ■

Proceeding as in [6], $\mathfrak{R}_{ij}(\cdot)$ is known to be a monotonically increasing function of z_{ij} , and thus \bar{M}_{ij} should also monotonically increase w.r.t. z_{ij} in either the case of $y_{ij} = 0$ or $y_{ij} = 1$. Accordingly, we first consider the boundary situation of the inequality constraint (16e), i.e., $\bar{M}_{ij} = M_i^o$, the minimum z_{ij} required by the association link between MU i and BS j to perform SemCom (denoted by z_{ij}^{SM}) and BitCom (denoted by z_{ij}^{BM}), respectively, can be

$$z_{ij}^{SM} = \frac{\mathfrak{R}_{ij}^{-1}(M_i^o / \tau_i)}{\log_2(1 + \bar{\gamma}_{ij})} \quad \text{and} \quad z_{ij}^{BM} = \frac{M_i^o}{\rho_{ij} \log_2(1 + \bar{\gamma}_{ij})}, \quad (17)$$

where $\mathfrak{R}_{ij}^{-1}(\cdot)$ indicates the inverse function of $\mathfrak{R}_{ij}(\cdot)$ w.r.t. z_{ij} . Likewise, in the context of (9) and (10), we can also obtain the constraint (16c)-based minimum z_{ij} (denoted by $z_{ij}^{S_\delta}$ and $z_{ij}^{B_\delta}$) and constraint (16d)-based minimum z_{ij} (denoted by $z_{ij}^{S_\theta}$ and $z_{ij}^{B_\theta}$) in their respective inequality boundary situations. It is worth pointing out here that the feasible $z_{ij}^{S_\delta}$ solution may not exist if $\delta_i^{S_\delta} > \delta_0$, while $\delta_i^{S_\delta}$ cannot be negative. In such a case, we set $z_{ij}^{S_\delta} = +\infty$ to avoid the possibility of the MU selecting the SemCom mode in the subsequent solution.

Afterward, our aim is to find the optimal $\mathbf{x}^* = \{x_{ij}^* \mid i \in \mathcal{U}, j \in \mathcal{J}\}$ and the optimal

$$\begin{aligned}G_{ij} &= \sum_{l=1}^F \alpha_{ij}^l \left[\sum_{k=0}^{l-1} \Pr\{D_{ij}=k\} \left(\sum_{f=F-l+k}^{\infty} (f+l-k-F) \Pr\{A'_i=f\} \right) + \left(\sum_{k=l}^{\infty} \Pr\{D_{ij}=k\} \right) \left(\sum_{f=F+1}^{\infty} (f-F) \Pr\{A'_i=f\} \right) \right] \\ &\quad + \alpha_{ij}^0 \sum_{k=F+1}^{\infty} (k-F) \Pr\{A'_i=k\}.\end{aligned}\quad (12)$$

$\mathbf{y}^* = \{y_{ij}^* \mid i \in \mathcal{U}, j \in \mathcal{J}\}$ by fixing each SemCom-associated z_{ij} term as $z_{ij}^{S_{th}} = \max\{z_{ij}^{S_M}, z_{ij}^{S_\delta}, z_{ij}^{S_\theta}\}$ and each BitCom-associated z_{ij} as $z_{ij}^{B_{th}} = \max\{z_{ij}^{B_M}, z_{ij}^{B_\delta}, z_{ij}^{B_\theta}\}$. As such, constraints (16c)-(16e) in the primal problem **P1** can be all removed, and then **P1** degenerates into

$$\mathbf{P1.1} : \max_{\mathbf{x}, \mathbf{y}} \sum_{i \in \mathcal{U}} \sum_{j \in \mathcal{J}} x_{ij} \left[y_{ij} \overline{M}_{ij}^{S_{th}} + (1 - y_{ij}) \overline{M}_{ij}^{B_{th}} \right] \quad (18)$$

$$\text{s.t.} \quad \sum_{i \in \mathcal{U}} x_{ij} \left[y_{ij} z_{ij}^{S_{th}} + (1 - y_{ij}) z_{ij}^{B_{th}} \right] \leq Z_j, \quad \forall j \in \mathcal{J}, \quad (18a)$$

$$(16a), (16f), \quad (18b)$$

where let $\overline{M}_{ij}^{S_{th}} = \tau_i \mathfrak{R}_{ij} \left(z_{ij}^{S_{th}} \log_2(1 + \overline{\gamma}_{ij}) \right)$ and $\overline{M}_{ij}^{B_{th}} = \rho_{ij} z_{ij}^{B_{th}} \log_2(1 + \overline{\gamma}_{ij})$, both are regarded as known constants.

Regarding **P1.1**, we incorporate constraint (18a) into its objective function (18) by associating Lagrange multipliers $\boldsymbol{\eta} = \{\eta_j \mid j \in \mathcal{J}\}$. The associated Lagrange function is presented in (19) at the bottom of this page, in which $\tilde{L}_\eta(\mathbf{x}, \mathbf{y})$ is defined for expression brevity. That way, the Lagrange dual problem of **P1.1** becomes

$$\mathbf{D1.1} : \min_{\boldsymbol{\eta}} H(\boldsymbol{\eta}) = g_{\mathbf{x}, \mathbf{y}}(\boldsymbol{\eta}) + \sum_{j \in \mathcal{J}} \eta_j Z_j \quad (20)$$

$$\text{s.t.} \quad \eta_j \geq 0, \quad \forall j \in \mathcal{J}, \quad (20a)$$

where

$$g_{\mathbf{x}, \mathbf{y}}(\boldsymbol{\eta}) = \sup_{\mathbf{x}, \mathbf{y}} \tilde{L}_\eta(\mathbf{x}, \mathbf{y}) \quad (21)$$

$$\text{s.t.} \quad (16a), (16f).$$

Notably, since (18) is convex and (18a) contains only linear and affine inequalities, according to the duality property [29], the above primal-dual transformation w.r.t. **D1.1** determines at least the best upper bound of **P1.1**. Hence, our focus now shifts to seeking \mathbf{x}^* and \mathbf{y}^* through solving problem (21) in an iterative fashion of updating $\boldsymbol{\eta}$ with a subgradient method [30].

Before that, all cross terms of \mathbf{x} and \mathbf{y} in $\tilde{L}_\eta(\mathbf{x}, \mathbf{y})$ need to be tackled for tractability, where $x_{ij}y_{ij}$ and $x_{ij}(1 - y_{ij})$ are the only two ways of crossing. Combined with constraint (16f), we first extend the original BS indicator set \mathcal{J} to $\mathcal{J}' = \{1, 2, \dots, J, J+1, J+2, \dots, 2J\}$ and define a new set of variables $\boldsymbol{\nu} = \{\nu_{ij'} \mid i \in \mathcal{U}, j' \in \mathcal{J}'\}$ w.r.t. (21), such that

$$\nu_{ij'} = \begin{cases} x_{ij'} y_{ij'}, & \text{if } j' \in \mathcal{J} = \{1, 2, \dots, J\}; \\ x_{i(j'-J)} (1 - y_{i(j'-J)}), & \text{if } j' \in \mathcal{J}' \setminus \mathcal{J}. \end{cases} \quad (22)$$

In parallel, we define another new set of constants $\boldsymbol{\xi} = \{\xi_{ij'} \mid i \in \mathcal{U}, j' \in \mathcal{J}'\}$ to characterize the coefficient of each $\nu_{ij'}$, i.e.,

$$\xi_{ij'} = \begin{cases} \overline{M}_{ij'}^{S_{th}} - \eta_{j'} z_{ij'}^{S_{th}}, & \text{if } j' \in \mathcal{J}; \\ \overline{M}_{i(j'-J)}^{B_{th}} - \eta_{(j'-J)} z_{i(j'-J)}^{B_{th}}, & \text{if } j' \in \mathcal{J}' \setminus \mathcal{J}. \end{cases} \quad (23)$$

As such, given the initial dual variable $\boldsymbol{\eta}$, problem (21) should be straightforwardly converted to

$$\mathbf{P1.2} : \max_{\boldsymbol{\nu}} \sum_{i \in \mathcal{U}} \sum_{j' \in \mathcal{J}'} \xi_{ij'} \nu_{ij'} \quad (24)$$

$$\text{s.t.} \quad \sum_{j' \in \mathcal{J}'} \nu_{ij'} = 1, \quad \forall i \in \mathcal{U}, \quad (24a)$$

$$\nu_{ij'} \in \{0, 1\}, \quad \forall (i, j') \in \mathcal{U} \times \mathcal{J}'. \quad (24b)$$

It is easily derived from **P1.2** that for any $i \in \mathcal{U}$, the optimal j' such that $\nu_{ij'} = 1$ is exactly the j' that enables the maximum $\xi_{ij'}$ compared with any other $j' \in \mathcal{J}'$. In other words, let $\hat{j}' = \arg \max_{j' \in \mathcal{J}'} \xi_{ij'}, \forall i \in \mathcal{U}$, we can determine \mathbf{x}^* and \mathbf{y}^* for each MU i and BS j in the HSB-Net by

$$\begin{cases} x_{ij}^* = 1, y_{ij}^* = 1, & \text{if } \hat{j}' \in \mathcal{J} \text{ and } j = \hat{j}'; \\ x_{ij}^* = 1, y_{ij}^* = 0, & \text{if } \hat{j}' \in \mathcal{J}' \setminus \mathcal{J} \text{ and } j = \hat{j}' - J; \\ x_{ij}^* = 0, & \text{otherwise.} \end{cases} \quad (25)$$

Afterward, the partial derivatives w.r.t. $\boldsymbol{\eta}$ in the objective function $H(\boldsymbol{\eta})$ in **D1.1** are set as the subgradient direction in each update iteration. Now suppose that in a certain iteration, e.g., iteration l , in line with constraint (20a), each η_j ($j \in \mathcal{J}$) is updated as the following rule:

$$\eta_j(l+1) = \max\{\eta_j(l) - \epsilon(l) \cdot \nabla H(\eta_j), 0\}, \quad (26)$$

where

$$\nabla H(\eta_j) = Z_j - \sum_{i \in \mathcal{U}} x_{ij} \left[y_{ij} z_{ij}^{S_{th}} + (1 - y_{ij}) z_{ij}^{B_{th}} \right], \quad (27)$$

and $\epsilon(l)$ denotes the stepsize of the update in iteration l . In general, the convergence of the subgradient descent method can be guaranteed with a properly preset stepsize [31].

Nevertheless, it is worth noting that the above solutions cannot always directly reach the optimality of **P1.1**, as the BA constraint (18a) may be violated at some BSs within each iteration. In this case, here we additionally adopt a preference list-based heuristic algorithm to project the solution obtained in each iteration back to the feasible set of (18a). To be concrete, \mathbf{x}^* and \mathbf{y}^* obtained by (22)-(27) are first leveraged to identify the index list of the BSs that violate (18a), denoted as $\tilde{\mathcal{J}} = \{j \mid j \in \mathcal{J}, \sum_{i \in \mathcal{U}} x_{ij}^* \left[y_{ij}^* z_{ij}^{S_{th}} + (1 - y_{ij}^*) z_{ij}^{B_{th}} \right] > Z_j\}$.

$$\begin{aligned} L(\mathbf{x}, \mathbf{y}, \boldsymbol{\eta}) &= \sum_{i \in \mathcal{U}} \sum_{j \in \mathcal{J}} x_{ij} \left[y_{ij} \overline{M}_{ij}^{S_{th}} + (1 - y_{ij}) \overline{M}_{ij}^{B_{th}} \right] + \sum_{j \in \mathcal{J}} \eta_j \left(Z_j - \sum_{i \in \mathcal{U}} x_{ij} \left[y_{ij} z_{ij}^{S_{th}} + (1 - y_{ij}) z_{ij}^{B_{th}} \right] \right) \\ &= \sum_{i \in \mathcal{U}} \sum_{j \in \mathcal{J}} \left[x_{ij} y_{ij} \left(\overline{M}_{ij}^{S_{th}} - \eta_j z_{ij}^{S_{th}} \right) + x_{ij} (1 - y_{ij}) \left(\overline{M}_{ij}^{B_{th}} - \eta_j z_{ij}^{B_{th}} \right) \right] + \sum_{j \in \mathcal{J}} \eta_j Z_j \\ &\triangleq \tilde{L}_\eta(\mathbf{x}, \mathbf{y}) + \sum_{j \in \mathcal{J}} \eta_j Z_j. \end{aligned} \quad (19)$$

Consider an arbitrary BS $\tilde{j} \in \tilde{\mathcal{J}}$, let $\mathcal{U}_{\tilde{j}} = \{i \mid i \in \mathcal{U}, x_{i\tilde{j}}^* = 1\}$ store all its current associated MUs, the MU that consumes the largest amount of bandwidth among all MUs can be found by

$$\hat{i} = \arg \max_{i \in \mathcal{U}_{\tilde{j}}} \left[y_{i\tilde{j}}^* z_{i\tilde{j}}^{S_{th}} + (1 - y_{i\tilde{j}}^*) z_{i\tilde{j}}^{B_{th}} \right]. \quad (28)$$

Next, we assume that MU \hat{i} has an initial variable set $\mathcal{J}'_i = \mathcal{J}'$, which can be reckoned as its UA and MS preference list pertinent to optimizing **P1.2**. Since the solution $(x_{i\tilde{j}}^*, y_{i\tilde{j}}^*)$ is obviously inapplicable due to the insufficient bandwidth resources at BS \tilde{j} , let the corresponding index $j' = \tilde{j}$ in its SemCom case or $j' = \tilde{j} + J$ in its BitCom case be removed from MU \hat{i} 's preference list \mathcal{J}'_i . That is,

$$\mathcal{J}'_i = \begin{cases} \mathcal{J}'_i \setminus \tilde{j}, & \text{if } y_{i\tilde{j}}^* = 1; \\ \mathcal{J}'_i \setminus (\tilde{j} + J), & \text{if } y_{i\tilde{j}}^* = 0, \end{cases} \quad (29)$$

whereby its current optimal \hat{j}' becomes

$$\hat{j}' = \arg \max_{j' \in \mathcal{J}'_i} \xi_{ij'}. \quad (30)$$

Calculating (25) again, we can update MU \hat{i} 's optimal UA and MS strategy $(x_{i\tilde{j}}^*, y_{i\tilde{j}}^*)$ over any BS $j \in \mathcal{J}$ as well as BS \tilde{j} 's UA list $\mathcal{U}_{\tilde{j}}$. After that, the satisfaction of constraint (18a) w.r.t. BS \tilde{j} should be rechecked, and even if it is still in violation, we can repeat the operations between (28) to (30) until (18a) is eventually met at BS \tilde{j} . Likewise, the above procedure can be applied to any other BS $j \in \tilde{\mathcal{J}}$ until the bandwidth constraints are fulfilled at all BSs after each iteration. In summary, by alternately updating (\mathbf{x}, \mathbf{y}) and $\boldsymbol{\eta}$ in combination with the proposed preference list-based heuristic algorithm, the UA and MS problems can be solved in the HSB-Net.

B. Optimal Solution for BA with Complexity Analysis

According to the obtained UA solution \mathbf{x}^* and MS solution \mathbf{y}^* , we aim to reallocate all bandwidth resources of each BS j ($\forall j \in \mathcal{J}$) to all its associated MUs, thus a total of S BA subproblems w.r.t. **P1** are constructed. Based on Proposition 2 alongside the preset bandwidth threshold $z_{ij}^{S_{th}}$ and $z_{ij}^{B_{th}}$, each BA subproblem of BS j is formulated as follows:

$$\mathbf{P1.3}_j : \max_{\mathbf{z}} \sum_{i \in \mathcal{U}_j^S} \bar{M}_{ij}^S + \sum_{i \in \mathcal{U}_j^B} \bar{M}_{ij}^B \quad (31)$$

$$\text{s.t.} \quad \sum_{i \in \mathcal{U}_j^S \cup \mathcal{U}_j^B} z_{ij} = Z_j, \quad (31a)$$

$$z_{ij} \geq z_{ij}^{S_{th}}, \quad \forall i \in \mathcal{U}_j^S, \quad (31b)$$

$$z_{ij} \geq z_{ij}^{B_{th}}, \quad \forall i \in \mathcal{U}_j^B, \quad (31c)$$

where $\mathcal{U}_j^S = \{i \mid i \in \mathcal{U}, x_{ij}^* = 1, y_{ij}^* = 1\}$ stands for the set of all SemCom-enabled MUs associated with BS j , and $\mathcal{U}_j^B = \{i \mid i \in \mathcal{U}, x_{ij}^* = 1, y_{ij}^* = 0\}$ represents the set of all BitCom-enabled MUs associated with BS j . Then given the convex property of $\mathfrak{R}_{ij}(\cdot)$ [6], we have the objective function and all constraints of each **P1.3_j** are convex, thereby efficient linear programming toolboxes such as CVPXY [32] can be directly applied to obtain the optimal BA solution for the HSB-Net.

TABLE I
SIMULATION PARAMETERS

Parameters	Values
Bandwidth budget of each BS (Z_j)	15 MHz [34]
Transmit power of each MU	20 dBm
Noise power	-111.45 dBm [35]
Path loss model	$34 + 40 \log(d \text{ [m]})$
Time slot length (T)	1 ms
Number of bits in each packet (L)	800 bits
Packet buffer size of PTQ (F)	20
Maximum average packet queuing latency threshold (δ_0)	20 ms
Maximum average packet loss ratio threshold (θ_0)	0.01

In terms of the computational complexity of the proposed solution, determining the minimum z_{ij} allocated to each potential UA link first requires $\mathcal{O}(F^2)$ complexity to compute the one-step state transition probability matrix of its PTQ as given in the proof of Proposition 1, hence $\mathcal{O}(UJF^2)$ complexity is needed for obtaining **P1.1**. Then, in each iteration of solving **D1.1**, the complexity is $\mathcal{O}(UJ^2)$ for at most J violated BSs to find their respective largest bandwidth-consumed MUs in a group of UJ variables. As such, if let V denote the required number of iterations that leads to convergence of **D1.1**, finalizing the UA and MS solutions needs a total of $\mathcal{O}(VUJ^2)$ complexity. Finally, since each **P1.3_j** can be solved by the linear programming method with complexity $\mathcal{O}(U^2)$ [33], the proposed wireless resource management solution has a polynomial-time overall complexity of $\mathcal{O}(UJ(F^2 + VJ + U))$.

V. NUMERICAL RESULTS AND DISCUSSIONS

In this section, numerical evaluations are conducted to demonstrate the performance of our proposed wireless resource management solution in the HSB-Net, where we employ Python 3.7-based PyCharm as the simulator platform and implement it in a workstation PC featuring the AMD Ryzen-9-7900X processor with 12 CPU cores and 128 GB RAM. To preserve generality, we first model a circular area with a radius of 300 meters, in which 200 MUs and 10 BSs are randomly dropped. Moreover, the SINR γ_{ij} follows a Gaussian distribution with standard deviation of 4 dB [16]. For brevity, some simulation parameters not mentioned in the context and their fixed values are summarized in Table I.

In SemCom-relevant settings, we simulate a general text transmission scenario to examine the proposed solution. Note that such performance test can also be accomplished with other content types like images or videos, and the reason we choose text is to leverage existing natural language processing models that have been well validated in SemCom-related works. Particularly, the Transformer in [2] is adopted as the unified semantic encoder for all SemCom links, and the PyTorch-based Adam optimizer is applied for model training with an initial learning rate of 0.001. Based on the public dataset extracted from the proceedings of European Parliament [36],

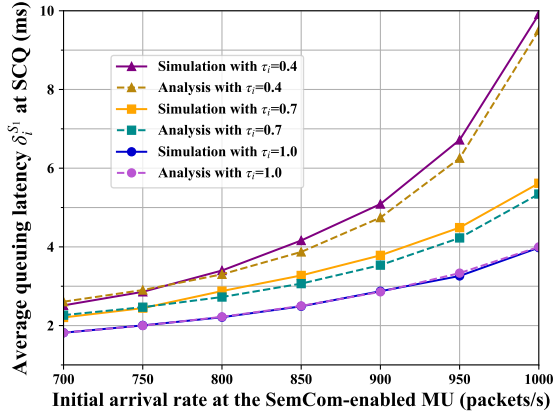


Fig. 3. Simulated and analytical results w.r.t. average queuing latency δ_i^{S1} at SCQ for varying packet arrival rates and average knowledge-matching degrees.

the expression of B2M function $\mathfrak{R}_{ij}(\cdot)$ at each SemCom link can be well approximated from extensive model tests [6].

As for the queuing modeling part, each MU's average knowledge-matching degree τ_i , minimum message rate threshold M_i^o , and BitCom-based B2M coefficient ρ_{ij} are randomly generated in the range of $0.6 \sim 1$, $50 \sim 100$, and $2 \times 10^{-5} \sim 2 \times 10^{-4}$, respectively. Besides, the average packet arrival rate λ_i is prescribed at 1000 packets/s for all MUs [37], while the average interpretation times of knowledge-matching and -mismatching packets in SCQ are considered as 8×10^{-4} and 1×10^{-3} s/packet, respectively. Furthermore, we set a dynamic stepsize of $\epsilon(l) = 1 \times 10^{-6}/l$ to update the Lagrange multipliers in (26), where the convergence of each trial can be always guaranteed. It is worth mentioning that all the above parameter values are set by default unless otherwise specified, and all subsequent numerical results are obtained by averaging over a sufficiently large number of trials.

For comparison purposes, here we employ four different resource management benchmarks in HSB-Nets by combining the max-SINR UA scheme (i.e., each MU is associated with the BS enabling the strongest SINR) with several differing MS and BA schemes, respectively. To the best of our knowledge, no existing work has proposed any benchmark solutions dedicatedly for MS, and therefore, two heuristic schemes are developed as MS baselines: (MS-I) A *knowledge matching degree-based* method, where each MU selects the SemCom mode when its knowledge matching degree is above a preset threshold (e.g., a threshold of 0.8 has been used in our simulations), and otherwise selects the BitCom mode; (MS-II) A *SINR-based* method, where each MU selects the BitCom mode when its SINR is above a preset threshold (e.g., a threshold of 6 dB has been used in our simulations), and otherwise selects the SemCom mode.¹⁰ In parallel, two typical BA schemes are adopted as baselines: (BA-I) The *water-filling* algorithm [38]; (BA-II) The *evenly-distributed* algorithm [39].

¹⁰The MS-I scheme is intuitive since the higher the knowledge matching degree, the better the semantic-related performance [6]. As for the MS-II scheme, this is because SemCom shows more powerful anti-noise capability in the low-SINR region [2], while BitCom ensures higher content transmission accuracy in the high-SINR region [4], thereby MS-II should be applicable.

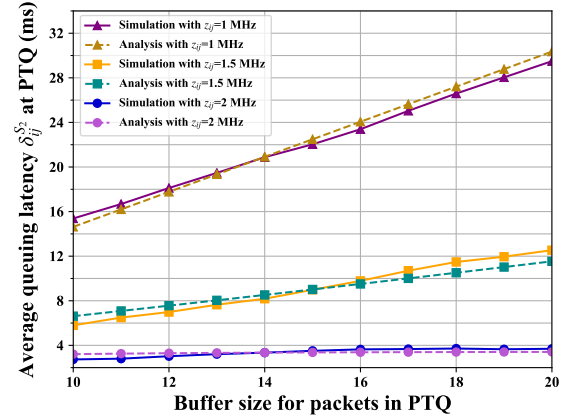


Fig. 4. Simulated and analytical results w.r.t. average queuing latency δ_{ij}^{S2} at PTQ for varying packet buffer sizes and allocated bandwidth resources.

A. Queuing Model Validation

For starters, we simulate the entire packet queuing processes for SCQ and PTQ at a SemCom-enabled MU with a default average knowledge-matching degree $\tau_i = 1.0$ and a default SINR $\gamma_{ij} = 0$ dB to validate the analytical accuracy of the derived queuing model. In detail, the analysis results are based on the direct computation of average packet queuing latency and packet loss ratio as in (11)-(14). In contrast, the simulation results are calculated by generating various randomized processes (including Poisson packet arrival, general-distribution based SCQ-packet departure and SINR-stochasticity based PTQ-packet departure) and averaging over 10,000 trials.

Figure 3 first depicts the average queuing latency δ_i^{S1} at SCQ by increasing the initial packet arrival intensity λ_i from 750 to 1050 packets/s, where $\tau_i = 0.4, 0.7$, and 1.0 are all taking into account. It is seen that the analytical curve basically agrees with the simulated one as λ_i grows, and the higher the τ_i , the closer the two latency curves in values. This can be explained by that the lower τ_i indicates the worse semantic inference capability for packet departure at SCQ, resulting in more uncertainty, i.e., higher fluctuation, on each randomly generated semantic-coding time. However, in our queuing analysis, the semantic-coding times of all knowledge-mismatching packets are simply approximated to have the same rate of $1/\mu_i^{Mis}$, which ignores the discrepancy between different knowledge-matching degrees, and thus rendering the numerical bias between simulated and analytical results in the lower τ_i region. Besides, the average queuing latency increases with the packet arrival rate in each case, which trend is obvious as the semantic-coding efficiency is fixed at SCQ.

Next, we compare the simulated and analytical results of PTQ in terms of its average queuing latency and packet loss ratio in Fig. 4 and Fig. 5, respectively, which are basically consistent in both cases. By varying PTQ's buffer size F from 10 to 22, Fig. 4 shows a moderate increasing trend in average queuing latency δ_{ij}^{S2} with different allocated bandwidth $z_{ij} = 1, 1.5$, and 2 MHz. This is logical since the buffer with a larger size is more likely to hold a long queue length, resulting in more average waiting time per packet according to (14). Moreover, it can be observed that the less the bandwidth

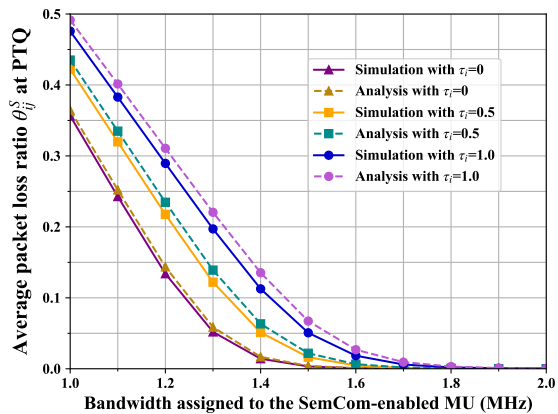


Fig. 5. Simulated and analytical results w.r.t. average packet loss ratio θ_{ij}^S at PTQ for varying bandwidth resources and knowledge-matching degrees.

assigned to the MU, the higher the $\delta_{ij}^{S_2}$ while the steeper the upward trend. Herein, the former phenomenon is reasonable due to the low packet departure rate as in (5). The latter is because that as the given z_{ij} grows, the rapid departure of packets gradually dominates the queuing process of PTQ, thereby the small changes in the buffer size could only have a slight impact on the rendered $\delta_{ij}^{S_2}$ performance.

Meanwhile, Fig. 5 presents the average packet loss ratio θ_{ij}^S at PTQ versus the allocated bandwidth z_{ij} under three average knowledge-matching degrees of $\tau_i = 0, 0.5, \text{ and } 1.0$, where the simulated results can always fit the analytical ones well. Specifically, the obtained θ_{ij}^S first decreases with z_{ij} , and then converges close to 0 when z_{ij} exceeds around 1.8 MHz. The rationale behind this is similar to Fig. 4, i.e., the packets arriving at the PTQ with a higher departure rate are less likely to be blocked. Furthermore, combined (7) with the setting of $\mu_i^{Mat} > \mu_i^{Mis}$, it is seen that the higher the τ_i , the higher the packet arrival rate of PTQ, and thus the greater the likelihood that its buffer tends to be full. Notably, the average packet loss ratio of PTQ and the overall queuing latency of both SCQ and PTQ should be taken into account together to meet the preset delay and reliability requirements. For instance, θ_{ij}^S can reach the threshold of $\theta_0 = 0.01$ by assigning 1.55 MHz bandwidth to the same MU with $\tau_i = 0.5$. However, even the default $\lambda_i = 1000$ packets/s will cause the queuing delay of 9.1 ms at SCQ and 11.5 ms at PTQ (i.e., the total of 20.6 ms) in the same case, which has exceeded the threshold $\delta_0 = 20$ ms.

B. Performance of the Proposed Solution

To validate our proposed resource management solution, we test the overall message throughput of HSB-Net under different numbers of BSs and MUs in Fig. 6 and Fig. 7, respectively, in comparison with the four benchmarks. As first elucidated in Fig. 6, by varying the number of BSs from 8 to 13, the message throughput performance of the proposed solution gradually increases from around 160 to 360 kmsg/s (1 kmsg/s = 1000 msg/s), and consistently outperforms these benchmarks. For example, a performance gain of the proposed solution is about 29.9 kmsg/s compared with the benchmark of Max-SINR plus MS-I plus BA-I and 102.6 kmsg/s compared

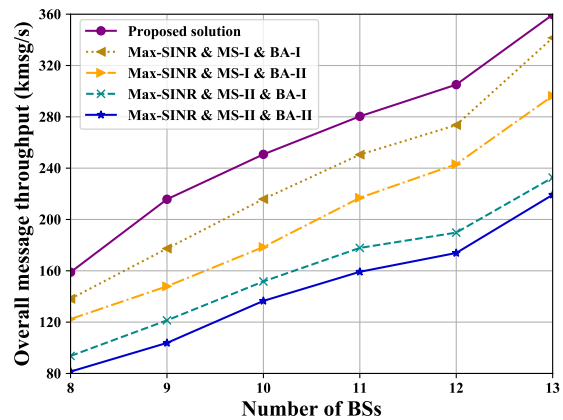


Fig. 6. Time-averaged overall message throughput (*kmsg/s*) versus different numbers of BSs in the HSB-Net.

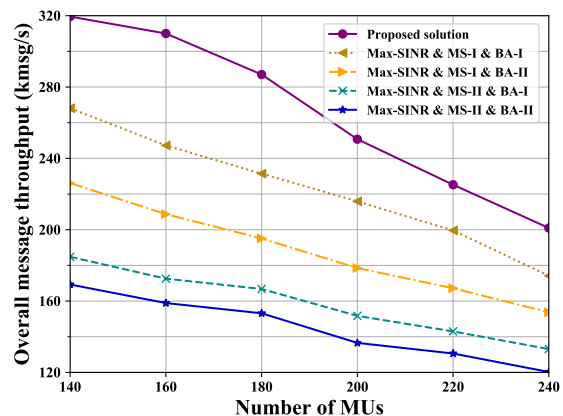


Fig. 7. Time-averaged overall message throughput (*kmsg/s*) versus different numbers of MUs in the HSB-Net.

with the benchmark of Max-SINR plus MS-II plus BA-I when 11 BSs are located in the HSB-Net. Here, such an uptrend is apparent since more BSs represent that more bandwidth resources are available for MUs to achieve higher message rates. Particularly in such an uplink scenario of HSB-Net, the increase in the number of BSs does not have any impact on channel interference, and hence a stable growth is observed.

By contrast, Fig. 7 demonstrates a downward trend of message throughput performance when rising the number of MUs from 140 to 240. To be concrete, the overall network performance is already saturated at the very beginning in holding 140 MUs and then deteriorates with the addition of MUs, as the effect of severe channel interference from excessive MUs starts to dominate the more availability of resources. In the meantime, it can be seen that our solution still surpasses all the four benchmarks with a significant performance gain. For instance, with 160 MUs in the HSB-Net, the proposed solution realizes a message throughput of about 310 kmsg/s, i.e., 1.5 times that of the Max-SINR plus MS-I plus BA-II scheme and 2 times that of the Max-SINR plus MS-II plus BA-II scheme.

In addition, we compare the message throughput performance with varying overall average knowledge-matching degree $\bar{\tau} = \frac{1}{U} \sum_{i \in U} \tau_i$ as shown in Fig. 8. Again, our solu-

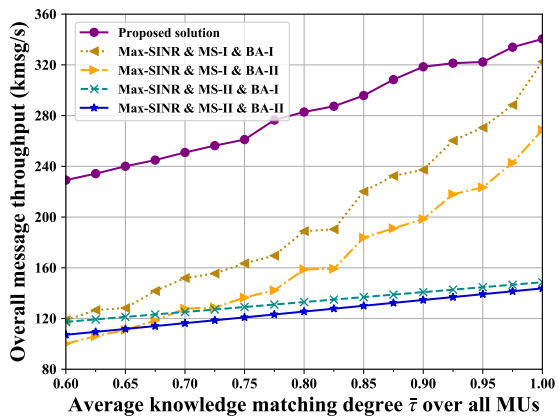


Fig. 8. Time-averaged overall message throughput ($kmsg/s$) versus different average knowledge-matching degrees over all 200 MUs in the HSB-Net.

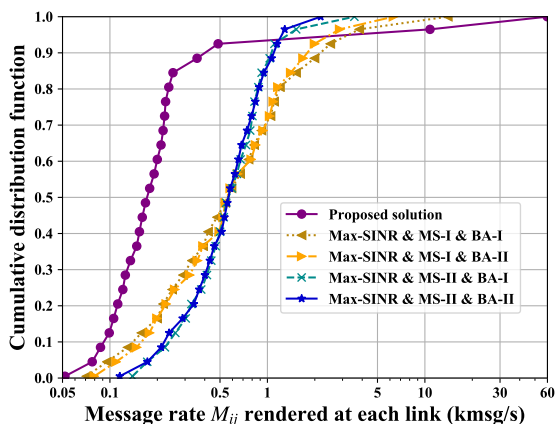


Fig. 9. The CDF of the message rate M_{ij} obtained by the associated link.

tion still outperforms these benchmarks with the considerable performance gain, especially in the low $\bar{\tau}$ region. Besides, a growing message throughput is observed by all solutions as $\bar{\tau}$ increases, and our solution and the MS-I scheme are more affected by changes in $\bar{\tau}$ compared to the MS-II. The former trend is intuitive since the larger $\bar{\tau}$ means that there is a greater likelihood for the HSB-Net having MUs with the high B2M transformation rates. The latter is first due to the message-throughput-priority design in our objective function (16), and therefore, our solution is more likely to generate more SemCom-enabled MUs with larger $\bar{\tau}$. Likewise, more SemCom-enabled MUs can exist in the same case according to the prescribed MS-I scheme, while the number of SemCom-enabled MUs is only affected by SINR in MS-II, and thus keeps stable irrespective of the change in $\bar{\tau}$.

Finally, the CDFs of the message rate M_{ij} rendered at all links are plotted in Fig. 9. Although most MUs in our solution only get the lower message rates compared with these benchmarks, this is reasonable since our optimization to **P1** focuses on the maximization for overall message throughput of all MUs in the HSB-Net. Hence, it can be interpreted as that the proposed solution choose to sacrifice user semantic fairness in favor of devoting more bandwidth resources to a smaller number of MUs with better average knowledge-

matching degrees, B2M transformation, and SINRs.

VI. CONCLUSIONS

In this paper, we investigated the wireless resource management problem in a novel yet practical network scenario, i.e., HSB-Net, where SemCom and BitCom modes are available for selection by all MUs. To measure SemCom and BitCom with the same performance metric, a B2M transformation function was first introduced to identify the message throughput of each associated link. Then, considering the unique semantic coding and knowledge matching mechanisms in SemCom, we modelled a two-stage tandem queuing system for the transmission of semantic packets, followed by the theoretical derivation for average packet loss ratio and queuing latency. On this basis, a joint optimization problem was formulated to maximize the overall message throughput of HSB-Net. Afterward, a Lagrange primal-dual method was employed and a preference list-based heuristic algorithm was developed to seek the optimal UA, MS, and BA solutions with the low computational complexity. Numerical results finally validated the accuracy of our queuing analysis and the performance superiority of our proposed solution in terms of overall message throughput compared with four different benchmarks.

This paper can serve as a pioneer work to offer valuable insights for follow-up research on hybrid SemCom and BitCom networks. Other relevant networking issues in the HSB-Net, such as communication mode switching or semantic fairness-driven power or resource block allocation, inevitably arise, which can treat this paper as the fundamental theoretical framework for reference. Since this work is limited to the long-term network optimization under known knowledge-matching degrees, the further problem about instantaneous decision-making for MS and BA in the unaware background knowledge condition could be a future research.

APPENDIX A

PROOF OF PROPOSITION 1

It is first found from (8) that given any queue length a at slot t (i.e., $Q_{ij}(t) = a$, $0 \leq a \leq F$), $Q_{ij}(t+1)$ is determined only by $A'_i(t)$ and $D_{ij}(t)$. Apparently, the stochastic $Q_{ij}(t)$ across all slots forms a discrete-time Markov process, herein we define $\omega_{ij}^{a \rightarrow b}(t) = \Pr\{Q_{ij}(t+1) = b \mid Q_{ij}(t) = a\}$ as its one-step state transition probability from state a at slot t to state b at slot $t+1$, $0 \leq b \leq F$. Since the PMFs of both $A'_i(t)$ and $D_{ij}(t)$ are independent of t , as mentioned earlier, we re-denote them by A'_i and D_{ij} for brevity, respectively. As such, $\omega_{ij}^{a \rightarrow b}(t)$ can be expressed as $\omega_{ij}^{a \rightarrow b}$ as well.

Having these, we have the one-step state transition probability matrix of SemCom-enabled PTQ as

$$\Omega_{ij} = \begin{bmatrix} \omega_{ij}^{0 \rightarrow 0} & \omega_{ij}^{0 \rightarrow 1} & \cdots & \omega_{ij}^{0 \rightarrow F} \\ \omega_{ij}^{1 \rightarrow 0} & \omega_{ij}^{1 \rightarrow 1} & \cdots & \omega_{ij}^{1 \rightarrow F} \\ \vdots & \vdots & \ddots & \vdots \\ \omega_{ij}^{F \rightarrow 0} & \omega_{ij}^{F \rightarrow 1} & \cdots & \omega_{ij}^{F \rightarrow F} \end{bmatrix}, \quad (32)$$

where each $\omega_{ij}^{a \rightarrow b}$ can be explicitly calculated in (33), placed at the bottom of the next page.

Further noticing that for the queue state transited from $Q_{ij}(t) = 0$ to $Q_{ij}(t+1) = 0$, the transition probability is

$$\begin{aligned} \Pr\{Q_{ij}(t+1) = 0 \mid Q_{ij}(t) = 0\} &= \Pr\{A'_i = 0\} \\ &= \exp(-\tau_i \mu_i^{Mat} T - (1 - \tau_i) \mu_i^{Mis} T) > 0, \end{aligned} \quad (34)$$

which proves that $Q_{ij}(t) = 0$ is aperiodic. Besides, combined with a fact that each $\omega_{ij}^{a \rightarrow b}$ is time independent and each $Q_{ij}(t)$ has a finite state space, $\{Q_{ij}(t) \mid t = 1, 2, \dots, N\}$ is time-homogeneous, irreducible, and aperiodic. Therefore, according to [40], there must be a unique steady-state probability vector $\alpha_{ij} = [\alpha_{ij}^0, \alpha_{ij}^1, \dots, \alpha_{ij}^F]^T$, which can be obtained by solving

$$\Omega_{ij}^T \alpha_{ij} = \alpha_{ij} \quad \text{and} \quad \sum_{k=0}^F \alpha_{ij}^k = 1. \quad (35)$$

This completes the proof.

APPENDIX B PROOF OF PROPOSITION 2

It is worth noting in the first place that here we only show the proof in the SemCom-enabled queuing model case of $y_{ij} = 1$ for exemplification (given any pair of MU i and BS j), since the proof in the BitCom case can be similarly derived based on their analogous modeling for PTQ. Notice that $\delta_{ij}^{S_1}$ is a known constant as in (11), $\delta_{ij}^{S_2}$ in (14) and θ_{ij}^S in (13) become the only two factors that z_{ij} can influence. Further combining that A'_i is irrelevant with z_{ij} as in (6), let us at first present a lemma of how z_{ij} relates the distribution of D_{ij} .

Lemma 1: The CDF of D_{ij} decreases as z_{ij} increases.

To prove Lemma 1, we first derive the CDF of D_{ij} from its PMF given in (5) as follows:

$$\begin{aligned} \Pr\{D_{ij} \leq k\} &= \sum_{f=0}^k \Pr\{D_{ij} = f\} \\ &= \Pr\left\{\gamma_{ij} \leq 2^{\frac{(k+1)L}{Tz_{ij}}} - 1\right\} - \Pr\left\{\gamma_{ij} \leq 2^{\frac{kL}{Tz_{ij}}} - 1\right\} \\ &\quad + \Pr\left\{\gamma_{ij} \leq 2^{\frac{kL}{Tz_{ij}}} - 1\right\} - \Pr\left\{\gamma_{ij} \leq 2^{\frac{(k-1)L}{Tz_{ij}}} - 1\right\} \\ &\quad + \Pr\left\{\gamma_{ij} \leq 2^{\frac{(k-1)L}{Tz_{ij}}} - 1\right\} - \Pr\left\{\gamma_{ij} \leq 2^{\frac{(k-2)L}{Tz_{ij}}} - 1\right\} \\ &\quad + \dots + \Pr\left\{\gamma_{ij} \leq 2^{\frac{L}{Tz_{ij}}} - 1\right\} - \Pr\{\gamma_{ij} \leq 0\} \\ &= \Pr\left\{\gamma_{ij} \leq 2^{\frac{(k+1)L}{Tz_{ij}}} - 1\right\} - \Pr\{\gamma_{ij} \leq 0\}, \quad k = 0, 1, 2, \dots, \end{aligned} \quad (36)$$

where slot index t is omitted from all notations associated with the SINR γ_{ij} for brevity due to its independence w.r.t. t

as aforementioned. Given arbitrary known CDF of γ_{ij} , which is independent with z_{ij} , we clearly have that $\Pr\{D_{ij} \leq k\}$ is a monotonically decreasing function of z_{ij} . This also implies that $\Pr\{D_{ij} \geq k\}$ monotonically increases w.r.t. z_{ij} .

Now, let us consider two complementary queuing state subspaces of queue length Q_{ij} , denoted by $\overleftarrow{\mathcal{F}}_c = \{0, 1, 2, \dots, c\}$ and $\overrightarrow{\mathcal{F}}_c = \{c+1, c+2, \dots, F\}$, $c = 0, 1, 2, \dots, F-1$. Given any current state c , it can only transit to either a smaller state in $\overleftarrow{\mathcal{F}}_c$ or a larger state in $\overrightarrow{\mathcal{F}}_c$ in the next step, and the probabilities of the two transition cases occurring sum to 1. According to the one-step transition probability $\omega_{ij}^{a \rightarrow b}$ expressed in (33), the probability of state c transiting to any state in $\overleftarrow{\mathcal{F}}_c$ should be computed by

$$\begin{aligned} &\omega_{ij}^{c \rightarrow 0} + \omega_{ij}^{c \rightarrow 1} + \dots + \omega_{ij}^{c \rightarrow c} \\ &= \Pr\{A'_i = 0\} + \Pr\{A'_i = 1\} \sum_{l=1}^{\infty} \Pr\{D_{ij} = l\} \\ &\quad + \Pr\{A'_i = 2\} \sum_{l=2}^{\infty} \Pr\{D_{ij} = l\} \\ &\quad + \dots + \Pr\{A'_i = c\} \sum_{l=c}^{\infty} \Pr\{D_{ij} = l\} \\ &= \Pr\{A'_i = 0\} + \sum_{k=1}^c \left(\Pr\{A'_i = k\} \sum_{l=k}^{\infty} \Pr\{D_{ij} = l\} \right) \\ &= \Pr\{A'_i = 0\} + \sum_{k=1}^c (\Pr\{A'_i = k\} \Pr\{D_{ij} \geq k\}). \end{aligned} \quad (37)$$

According to Lemma 1, (37) is clearly a monotonically increasing function of z_{ij} due to its $\Pr\{D_{ij} \geq k\}$ term. In other words, we have that the probability of any fixed state c transiting to a state in $\overrightarrow{\mathcal{F}}_c$ monotonically decreases w.r.t. z_{ij} . Further combined with the obtained steady-state probability vector α_{ij} , if denoting the cumulative distribution of the queuing system staying in the state space $\overleftarrow{\mathcal{F}}_c$ as $W_{ij}^{(c)} = \sum_{l=0}^c \alpha_{ij}^l$, $W_{ij}^{(c)}$ is increasing w.r.t. z_{ij} for any c as well.

By leveraging a fact that $W_{ij}^{(F)} = 1$, let us first rephrase the numerator term of $\delta_{ij}^{S_2}$ in (14) as follows:

$$\begin{aligned} \mathbb{E}[Q_{ij}(t)] &= \sum_{k=1}^F \alpha_{ij}^k + \sum_{k=2}^F \alpha_{ij}^k + \dots + \sum_{k=F-1}^F \alpha_{ij}^k + \alpha_{ij}^F \\ &= (1 - W_{ij}^{(0)}) + (1 - W_{ij}^{(1)}) + \dots + (1 - W_{ij}^{(F-1)}), \end{aligned} \quad (38)$$

whereby the conclusion that $\mathbb{E}[Q_{ij}(t)]$ is monotonically decreasing w.r.t. z_{ij} holds.

$$\omega_{ij}^{a \rightarrow b} = \begin{cases} \Pr\{A'_i = b\}, & \text{if } a = 0, 1 \leq b \leq F-1; \\ \sum_{k=F}^{\infty} \Pr\{A'_i = k\}, & \text{if } a = 0, b = F; \\ \Pr\{A'_i = 0\} \sum_{k=a}^{\infty} \Pr\{D_{ij} = k\}, & \text{if } 0 \leq a \leq F, b = 0; \\ \Pr\{A'_i = b\} \sum_{k=a}^{\infty} \Pr\{D_{ij} = k\} + \sum_{l=0}^{b-1} \Pr\{A'_i = l\} \Pr\{D_{ij} = a - b + l\}, & \text{if } 1 \leq a \leq F, 1 \leq b \leq a, b \neq F; \\ \Pr\{A'_i = b\} \sum_{k=a}^{\infty} \Pr\{D_{ij} = k\} + \sum_{l=0}^{a-1} \Pr\{D_{ij} = l\} \Pr\{A'_i = b - a + l\}, & \text{if } 1 \leq a < b \leq F-1; \\ \sum_{k=b}^{\infty} \Pr\{A'_i = k\} \sum_{l=a}^{\infty} \Pr\{D_{ij} = l\} + \sum_{l=0}^{a-1} (\Pr\{D_{ij} = l\} \sum_{k=b-a+l}^{\infty} \Pr\{A'_i = k\}), & \text{if } 1 \leq a \leq F, b = F. \end{cases} \quad (33)$$

Regarding θ_{ij}^S in (12), which is also served as the key term in the denominator of $\delta_{ij}^{S_2}$, we restructure the formula by highlighting all its implicit terms that transform to $\Pr\{D_{ij} \leq k\}$ and $W_{ij}^{(c)}$, and obtain

$$G_{ij} = \sum_{f=1}^F \Pr\{A'_i = f\} \left[\sum_{k=0}^{f-1} \Pr\{D_{ij} \leq k\} \left(1 - W_{ij}^{(F-f+k)}\right) \right] + \sum_{f=F+1}^{\infty} \Pr\{A'_i = f\} \left[(f-F) + \sum_{k=0}^{F-1} \Pr\{D_{ij} \leq k\} \left(1 - W_{ij}^{(k)}\right) \right]. \quad (39)$$

Again employing Lemma 1, we have that G_{ij} monotonically decreases w.r.t. z_{ij} , thereby θ_{ij}^S and $\delta_{ij}^{S_2}$ should have the same decreasing property. Finally, note that $\delta_{ij}^S = \delta_{ij}^{S_1} + \delta_{ij}^{S_2} \geq \delta_{ij}^{S_1} > 0$ always holds in practice, δ_{ij}^S must be monotonically non-increasing w.r.t. z_{ij} , which completes the proof.

REFERENCES

- [1] P. Zhang, W. Xu, H. Gao, K. Niu, X. Xu, X. Qin, C. Yuan, Z. Qin, H. Zhao, J. Wei, *et al.*, "Toward wisdom-evolutionary and primitive-concise 6G: A new paradigm of semantic communication networks," *Engineering*, vol. 8, no. 1, pp. 60–73, 2022.
- [2] H. Xie, Z. Qin, G. Y. Li, and B.-H. Juang, "Deep learning enabled semantic communication systems," *IEEE Transactions on Signal Processing*, vol. 69, pp. 2663–2675, 2021.
- [3] H. Zhang, H. Wang, Y. Li, K. Long, and A. Nallanathan, "DRL-driven dynamic resource allocation for task-oriented semantic communication," *IEEE Transactions on Communications*, vol. 71, no. 7, pp. 3992–4004, 2023.
- [4] L. Xia, Y. Sun, C. Liang, D. Feng, R. Cheng, Y. Yang, and M. A. Imran, "WiservR: Semantic communication enabled wireless virtual reality delivery," *IEEE Wireless Communications*, vol. 30, no. 2, pp. 32–39, 2023.
- [5] L. Xia, Y. Sun, C. Liang, L. Zhang, M. A. Imran, and D. Niyato, "Generative AI for semantic communication: Architecture, challenges, and outlook," *arXiv preprint arXiv:2308.15483*, 2023.
- [6] L. Xia, Y. Sun, D. Niyato, X. Li, and M. A. Imran, "Joint user association and bandwidth allocation in semantic communication networks," *IEEE Transactions on Vehicular Technology*, pp. 1–13, 2023.
- [7] J. Bao, P. Basu, M. Dean, C. Partridge, A. Swami, W. Leland, and J. A. Hendler, "Towards a theory of semantic communication," in *2011 IEEE Network Science Workshop*. IEEE, 2011, pp. 110–117.
- [8] P. Basu, J. Bao, M. Dean, and J. Hendler, "Preserving quality of information by using semantic relationships," *Pervasive and Mobile Computing*, vol. 11, pp. 188–202, 2014.
- [9] R. Carnap and Y. Bar-Hillel, "An outline of a theory of semantic information," 1952.
- [10] J. Liu, S. Shao, W. Zhang, and H. V. Poor, "An indirect rate-distortion characterization for semantic sources: General model and the case of Gaussian observation," *IEEE Transactions on Communications*, vol. 70, no. 9, pp. 5964–5959, 2022.
- [11] H. Xie and Z. Qin, "A lite distributed semantic communication system for Internet of Things," *IEEE Journal on Selected Areas in Communications*, vol. 39, no. 1, pp. 142–153, 2020.
- [12] Z. Yang, M. Chen, Z. Zhang, and C. Huang, "Energy Efficient Semantic Communication Over Wireless Networks With Rate Splitting," *IEEE Journal on Selected Areas in Communications*, vol. 41, no. 5, pp. 1484–1495, 2023.
- [13] R. Kaewpuang, M. Xu, W. Y. B. Lim, D. Niyato, H. Yu, J. Kang, and X. Shen, "Cooperative resource management in quantum key distribution (QKD) networks for semantic communication," *IEEE Internet of Things Journal*, vol. 11, no. 3, pp. 4454–4469, 2024.
- [14] L. Xia, Y. Sun, D. Niyato, D. Feng, L. Feng, and M. A. Imran, "xURLLC-aware service provisioning in vehicular networks: A semantic communication perspective," *IEEE Transactions on Wireless Communications*, 2023.
- [15] C. Guo, L. Liang, and G. Y. Li, "Resource allocation for vehicular communications with low latency and high reliability," *IEEE Transactions on Wireless Communications*, vol. 18, no. 8, pp. 3887–3902, 2019.
- [16] A. L. Moustakas and P. Kazakopoulos, "SINR statistics of correlated MIMO linear receivers," *IEEE Transactions on Information Theory*, vol. 59, no. 10, pp. 6490–6500, 2013.
- [17] R. C. Merkle, "Secure communications over insecure channels," *Communications of the ACM*, vol. 21, no. 4, pp. 294–299, 1978.
- [18] F. Meshkati, H. V. Poor, S. C. Schwartz, and R. V. Balan, "Energy-efficient resource allocation in wireless networks with quality-of-service constraints," *IEEE Transactions on Communications*, vol. 57, no. 11, pp. 3406–3414, 2009.
- [19] L. Xu and W. Zhuang, "Energy-efficient cross-layer resource allocation for heterogeneous wireless access," *IEEE Transactions on Wireless Communications*, vol. 17, no. 7, pp. 4819–4829, 2018.
- [20] G. Ding, J. Yuan, G. Yu, and Y. Jiang, "Two-timescale resource management for ultrareliable and low-latency vehicular communications," *IEEE Transactions on Communications*, vol. 70, no. 5, pp. 3282–3294, 2022.
- [21] Y. Wang, X. Tao, Y. T. Hou, and P. Zhang, "Effective capacity-based resource allocation in mobile edge computing with two-stage tandem queues," *IEEE Transactions on Communications*, vol. 67, no. 9, pp. 6221–6233, 2019.
- [22] C.-H. Wu, M. E. Lewis, and M. Veatch, "Dynamic allocation of reconfigurable resources in a two-stage tandem queueing system with reliability considerations," *IEEE Transactions on Automatic Control*, vol. 51, no. 2, pp. 309–314, 2006.
- [23] P. Li, D. Paul, R. Narasimhan, and J. Cioffi, "On the distribution of SINR for the MMSE MIMO receiver and performance analysis," *IEEE Transactions on Information Theory*, vol. 52, no. 1, pp. 271–286, 2005.
- [24] X. Luo, H.-H. Chen, and Q. Guo, "Semantic communications: Overview, open issues, and future research directions," *IEEE Wireless Communications*, pp. 1–10, 2022.
- [25] F. Pollaczek, "Über eine Aufgabe der Wahrscheinlichkeitstheorie. I," *Mathematische Zeitschrift*, vol. 32, no. 1, pp. 64–100, 1930.
- [26] S. M. Ross, *Introduction to Probability Models*. Academic Press, 2014.
- [27] J. D. Little and S. C. Graves, "Little's law," *Building Intuition: Insights from Basic Operations Management Models and Principles*, vol. 52, no. 1, pp. 81–100, 2008.
- [28] S. Burer and A. N. Letchford, "Non-convex mixed-integer nonlinear programming: A survey," *Surveys in Operations Research and Management Science*, vol. 17, no. 2, pp. 97–106, 2012.
- [29] S. Boyd, S. P. Boyd, and L. Vandenberghe, *Convex Optimization*. Cambridge University Press, 2004.
- [30] S. Boyd, L. Xiao, and A. Mutapic, "Subgradient methods," *Lecture Notes of EE392o, Stanford University, Autumn Quarter*, vol. 2004, pp. 2004–2005, 2003.
- [31] W. Jiang, G. Feng, and S. Qin, "Optimal cooperative content caching and delivery policy for heterogeneous cellular networks," *IEEE Transactions on Mobile Computing*, vol. 16, no. 5, pp. 1382–1393, 2016.
- [32] S. Diamond and S. Boyd, "CVXPY: A Python-embedded modeling language for convex optimization," *The Journal of Machine Learning Research*, vol. 17, no. 1, pp. 2909–2913, 2016.
- [33] Y. T. Lee, Z. Song, and Q. Zhang, "Solving empirical risk minimization in the current matrix multiplication time," in *Conference on Learning Theory*. PMLR, 2019, pp. 2140–2157.
- [34] L. Xu, A. Nallanathan, J. Yang, and W. Liao, "Power and bandwidth allocation for cognitive heterogeneous multi-homing networks," *IEEE Transactions on Communications*, vol. 66, no. 1, pp. 394–403, 2017.
- [35] H. Boostanimehr and V. K. Bhargava, "Unified and distributed QoS-driven cell association algorithms in heterogeneous networks," *IEEE Transactions on Wireless Communications*, vol. 14, no. 3, pp. 1650–1662, 2014.
- [36] P. Koehn, *et al.*, "Europarl: A parallel corpus for statistical machine translation," in *MT Summit*, vol. 5. Citeseer, 2005, pp. 79–86.
- [37] Y. Song, K. W. Sung, and Y. Han, "Impact of packet arrivals on Wi-Fi and cellular system sharing unlicensed spectrum," *IEEE Transactions on Vehicular Technology*, vol. 65, no. 12, pp. 10204–10208, 2016.
- [38] P. He, L. Zhao, S. Zhou, and Z. Niu, "Water-filling: A geometric approach and its application to solve generalized radio resource allocation problems," *IEEE transactions on Wireless Communications*, vol. 12, no. 7, pp. 3637–3647, 2013.
- [39] Q. Ye, B. Rong, Y. Chen, M. Al-Shalash, C. Caramanis, and J. G. Andrews, "User association for load balancing in heterogeneous cellular networks," *IEEE transactions on Wireless Communications*, vol. 12, no. 6, pp. 2706–2716, 2013.
- [40] G. Bolch, S. Greiner, H. De Meer, and K. S. Trivedi, *Queueing Networks and Markov Chains: Modeling and Performance Evaluation with Computer Science Applications*. John Wiley & Sons, 2006.